Civil Engineering Infrastructures Journal 2022, 55(1): 43-58
DOI: 10.22059/CEIJ.2021.308759.1702

RESEARCH PAPER

Simulation of Near-Fault Seismic Ground Motions of 03 November, 2002 Denali Earthquake Using Modified Semi-Empirical Approach

Rajaram, C.[1*] and Pradeep Kumar, R.[2]

[1] Associate Professor, School of Civil Engineering, Rajeev Gandhi Memorial College of Engineering and Technology, Nandyal, India.
[2] Professor, Earthquake Engineering Research Centre, International Institute of Information Technology, Hyderabad, India.

Received: 23 Aug. 2020; Revised: 17 Aug. 2021; Accepted: 30 Aug. 2021

ABSTRACT: An effective earthquake (Mw 7.9) struck Alaska on 3 November, 2002. It ruptured 340 km along three faults namely, the Susitna Glacier, Denali and Totschunda faults in central Alaska. The earthquake was recorded at 23 stations in Alaska and the Peak Ground Acceleration (PGA) of 0.32g was recorded at station PS10, which was located 3 km from the fault rupture. In this study, strike-slip Denali fault has been considered for studying the characteristics of ground motions through modified semi-empirical approach. The ground motion records of the 2002 Denali earthquake are generated through MATLAB code. The results revealed that modified semi-empirical approach is fairly good in agreement with observed ground motion records at all stations. A perfect match is observed between Fourier amplitude spectra of simulated and observed ground motions at PS09 and CARLO stations. A good match is observed between elastic response spectra of observed and simulated ground motions.

Keywords: Denali Earthquake, Fourier Amplitude Spectrum, Ground Motion Prediction Equation, Synthetic Accelerogram.

1. Introduction

A massive earthquake of magnitude M7.9 occurred on 3 November 2002 at a depth of 4.2 km in central Alaska (AEIC, 2003). The rupture started at 48 km of Susitna Glacier fault, propagated towards 226 km of Denali fault and terminated at 66 km of Totsunda fault (Lin et al., 2020). The Trans-Alaska pipeline pump station 10 located 3 km from surface rupture recorded a peak ground acceleration of 0.32g. It was the strongest event ever recorded in the interior of Alaska. Fortunately, no fatalities recorded in the densely populated region. The Denali fault behavior is similar to that of the San Andreas fault system in California (Uenishi, 2017). The rupture history of Denali earthquake was analyzed using teleseismic P-wave data to understand the rupture initiation and the behavior of Denali fault (Ozacar et al., 2004; Yousef and Jonathan 2020). Past studies showed that this earthquake was initiated by an unknown thrust fault propagating towards east (Kikuchi and Yamanaka, 2002; Lin et al., 2020). Echelon features were also observed on the surface during rupture along the

* Corresponding author E-mail: rajaram.chenna@research.iiit.ac.in

Denali fault.

2. Description of Denali Earthquake

2.1. Tectonic Setting and Fault Motion

The 2002 Denali earthquake happened due to interaction between Pacific plate and North American plate. This thrust motion was the cause of the 1964 Alaska earthquake (M9.2), which was the largest inland seismic event in central Alaska (Lin et al., 2020). The mainshock originated about 20 km towards east of the foreshock. The strike and dip angles of Susitna Glacier fault were 262^0 and 48^0, respectively. The strike angle of Denali fault was 102^0 with vertical dip. The scrap height of Susitna Glacier fault measured was about 4.0 m. The average and peak slip of Denali fault were 2.14 and 9.94 m, respectively (Dreger, 2003). The average slip of Totschunda fault was 1.7 m. Figure 1 shows the location of the Denali fault and the epicenter of the 3 November 2002 Denali earthquake. The geophysical parameters of the earthquake are shown in Table 1.

2.2. Seismicity of the Denali Fault

A foreshock of M6.7 occurred on 23 October 2002 in Nenana Mountain range before a main shock. Around 15,000 aftershocks were occurred during first two months after the main shock (AEIC, 2003). The first earthquake documented was the one on Sanak and Shumagin Islands, south of the Alaskan Peninsula, in July 1788. Alaska experienced few major-to-great earthquakes from 1899 to 1969. Among them, 1946 Aleutian Islands (M8.6), and 1964 Alaskan earthquake (M9.2) caused extensive property damage and topographic changes (USGS, 1964). The earthquake on the Denali fault prior to the 2002 was the magnitude 7.2 that occurred in July 1912 (Rachkovski et al., 2003). Since no seismographs and no reports were available in Alaska at that time, the location of the 1912 shock is uncertain. Figure 1 shows past seismicity of Alaskan region since 1898. The list of past major earthquakes experienced by Alaska since 1899 is shown in Table 2.

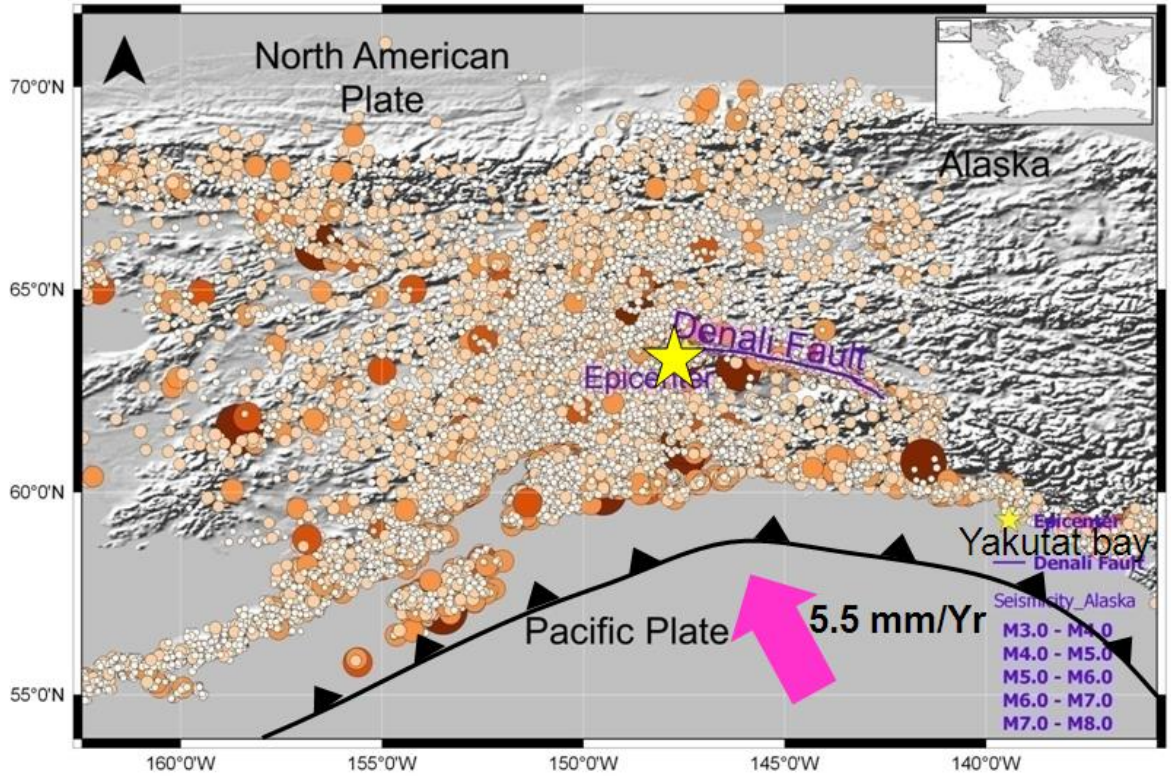

Fig. 1. Location of Denali fault, epicenter (denoted with star) of 3 November 2002 Denali earthquake. Past seismicity of Alaska in the region of Denali since 1898 (Data Source: USGS, 2013; AEIC, 2013)

Table 1. Geophysical parameters of 3 November 2002, Denali earthquake

Parameters	Values
Magnitude	7.9
Type of fault	Strike-slip fault
Name of fault	Denali fault
Seismic moment (Nm)	8.45×10^{20}
Strike angle	102^{o} (Dreger, 2003)
Dip angle	90^{o} (Dreger, 2003)
Shear wave velocity, β (km/s)	3.55 (Dreger, 2003)
Rupture velocity, V_r (km/s)	2.84
Average and peak slip (m)	2.14 and 9.94 m
Slip rise time (s)	2-4
Seismic moment, M_o (Nm)	8.45×10^{20} (Dreger, 2003)
Shear modulus (N/m^2)	3.52×10^{10}
Material density (kg/m^3)	2790

Table 2. Major to great earthquakes experienced by Alaska in past since 1899 (Source: USGS, 2013)

S No.	Date	Magnitude	Location
1	10 September 1899	8.6	Yakutat bay
2	09 October 1900	7.7	Kodiak island
3	22 July 1937	7.3	Southeast of Fairbanks
4	15 October 1947	7.3	Southeast of Fairbanks
5	07 April 1958	7.3	Central Alaska
6	28 March 1964	9.2	Great Alaska
7	04 February 1965	8.7	Rat island
8	03 October 2002	7.9	Denali
9	23 June 2014	7.9	Aleutian islands

3. Literature Review

The wave propagation theory was used to develop artificial ground motions using composite source method and the method yields good results for 1991 Uttarkashi earthquake (Anderson, 2015). However, the main drawback of the method is it requires geophysical parameters such as fault plane solutions, stress drop etc. The availability of these parameters is difficult for a site of interest. Empirical Green's function method suites to develop ground motion records, if small event accelerograms exist in the study area. This method is validated with a M8.5 scenario earthquake and yields good results (Krishnavajjhala, 2021). The stochastic simulation method fails to simulate near-field ground motions of large earthquakes.

The current study considers semi-empirical method to simulate ground motion records for the 2002 Denali earthquake. A step-by-step procedure of the method is described in the following section. This method yields good results for ground motions of several earthquakes such as 1999 Chi-Chi earthquake (Rajaram, 2016), 1991 Uttarkashi earthquake, 2009 Bhutan earthquake (Sandeep et al., 2017), 2013 Doda earthquake (Rajaram and Pradeep, 2016) and 2013 Pakistan earthquake (Rajaram and Pradeep, 2020). The main objective of the study is to find out the efficacy of the method for Alaska region. For this purpose, the 2002 Denali earthquake of magnitude 7.9 have been chosen to generate accelerograms. In this analysis, the Ground Motion Prediction Equation (GMPE), geophysical parameters are derived with the Alaskan data during 1971-2014.

3.1. Observed Ground Motions

Around 42 seismic stations digitally recorded the Denali earthquake operated by various organizations (AEIC, UoAF, USGS, ATWC and Alyeska). More than 50% of seismic stations are located in Anchorage metropolitan region. The sampling frequency for R109 and CARLO seismic stations is 100 Hz and for other stations, it is 200 Hz (Tadahiro et al., 2016).

The locations of ground motion records are taken from Pacific Earthquake Engineering Research are shown in Figure 2. The current study addresses Denali fault alone due to complexity of the fault. Near-field ground motions records at stations PS10, PS09, CARLO and R109 are considered in this study and its ground motion records are shown in Figure 3. The parameters such as, location of seismic stations relative to the fault and epicenter, horizontal and vertical fault slip and spectral decay frequency are shown in Table 3. The PGA values of Fault Normal (FN) and Fault Parallel (FP) components are shown in Table 4. The Fourier amplitude spectra and acceleration response spectra at all stations are shown in Figures 4 and 5. Each seismic station ground motion characteristics are described below.

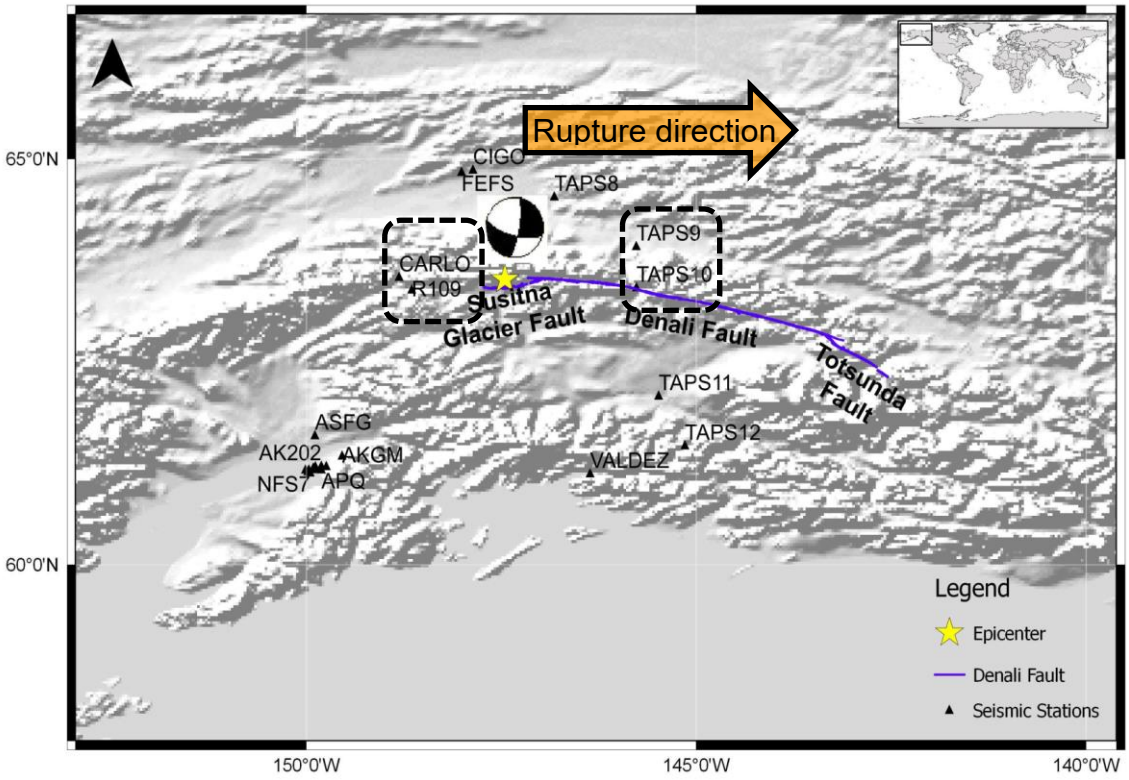

Fig. 2. Locations of the strong ground motion stations that recorded during 2002 Denali earthquake (Data Source: USGS, 2013; AEIC, 2013)

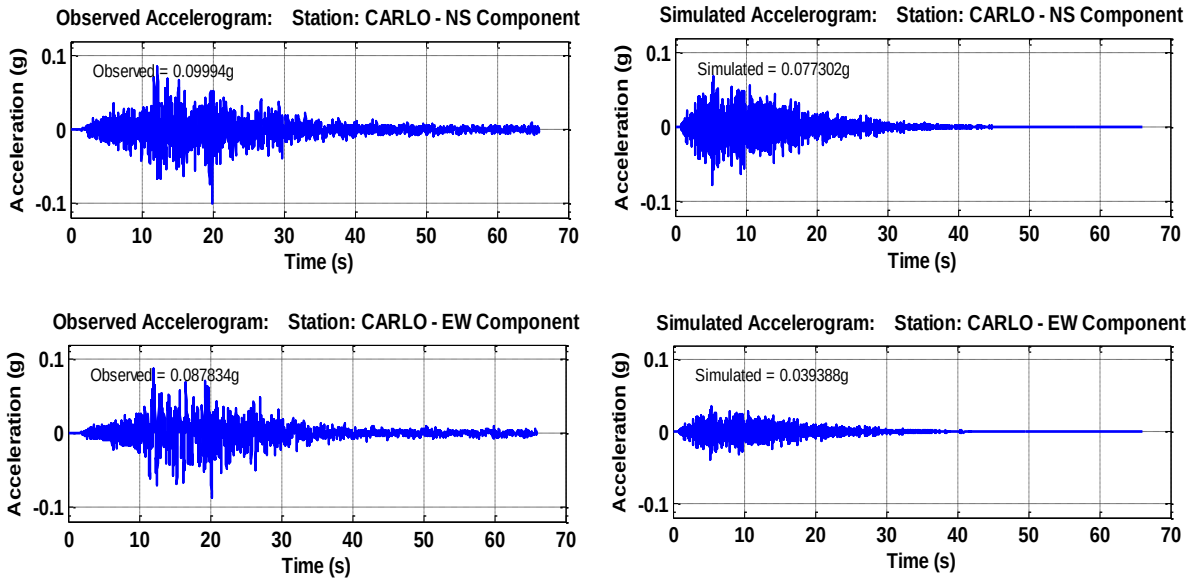

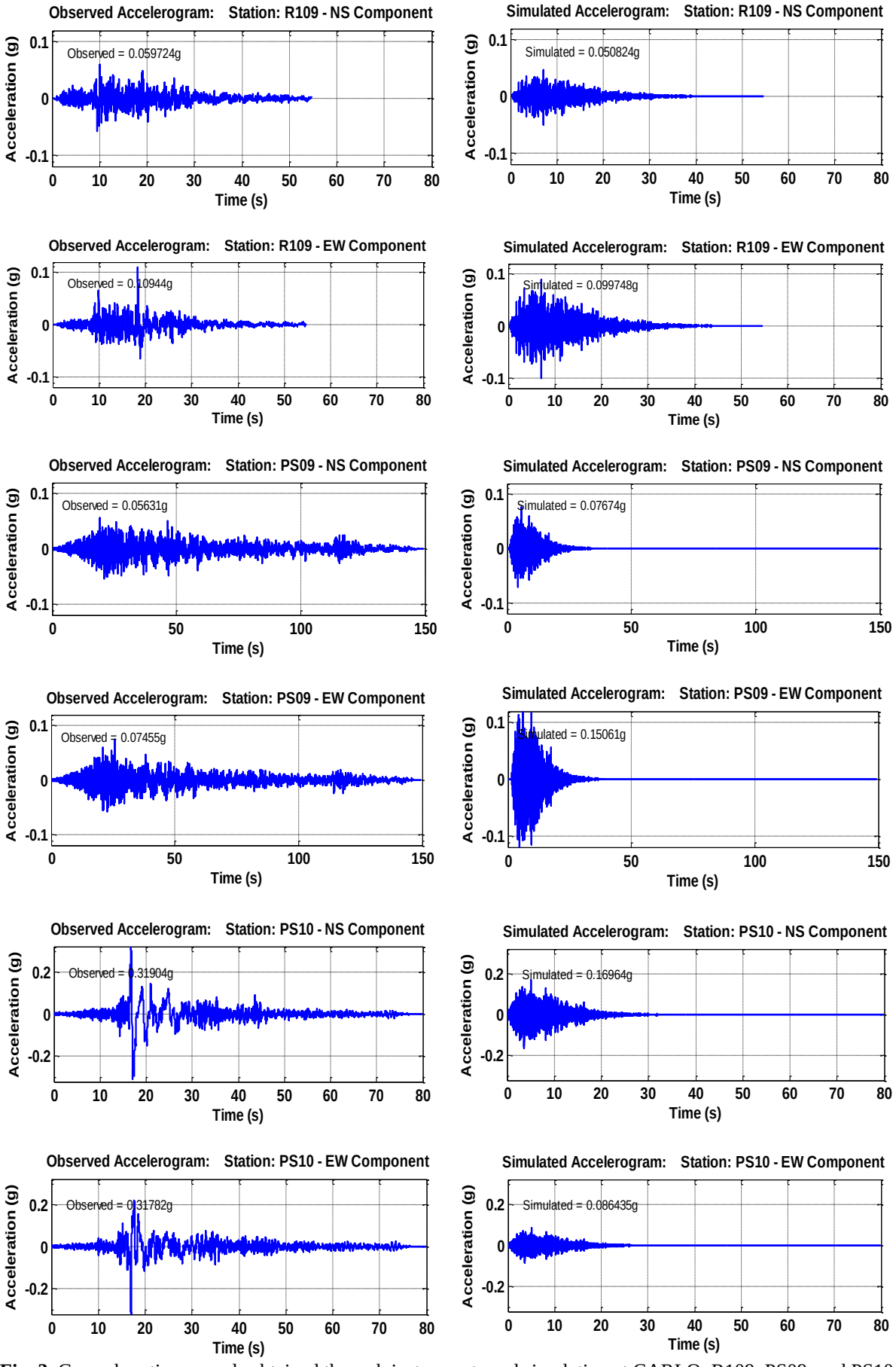

Fig. 3. Ground motion records obtained through instruments and simulation at CARLO, R109, PS09, and PS10 stations of the 2002 Denali earthquake (Data Source: SMVDC, 2013)

Table 3. Location of seismic stations relative to the fault and epicenter, horizontal and vertical fault slip and frequency decay of 3 November 2002, Denali earthquake

Station	Latitude (°N)	Longitude (°W)	Epicentral distance (km)	Distance from fault (km)	Horizontal fault slip (m)	Vertical fault slip (m)	Spectral decay frequency (Hz)
PS10	63.423	145.765	85.0	3.0	5.6	1.6	1.0
PS09	63.931	145.768	94.0	56.0	6.0	1.48	5.0
CARLO	63.551	148.809	68.0	59.0	3.9	1.06	5.0
R109	63.395	148.646	63.0	49.0	2.28	0.49	2.0

Table 4. Comparison of between observed, and simulated ground motions of 03 November 2002, Denali earthquake

Station	Observed PGA (g)		Simulated PGA (g)	
	FN	FP	FN	FP
PS10	0.319	0.317	0.17	0.086
PS09	0.056	0.074	0.076	0.15
CARLO	0.099	0.08	0.077	0.04
R109	0.06	0.109	0.05	0.10

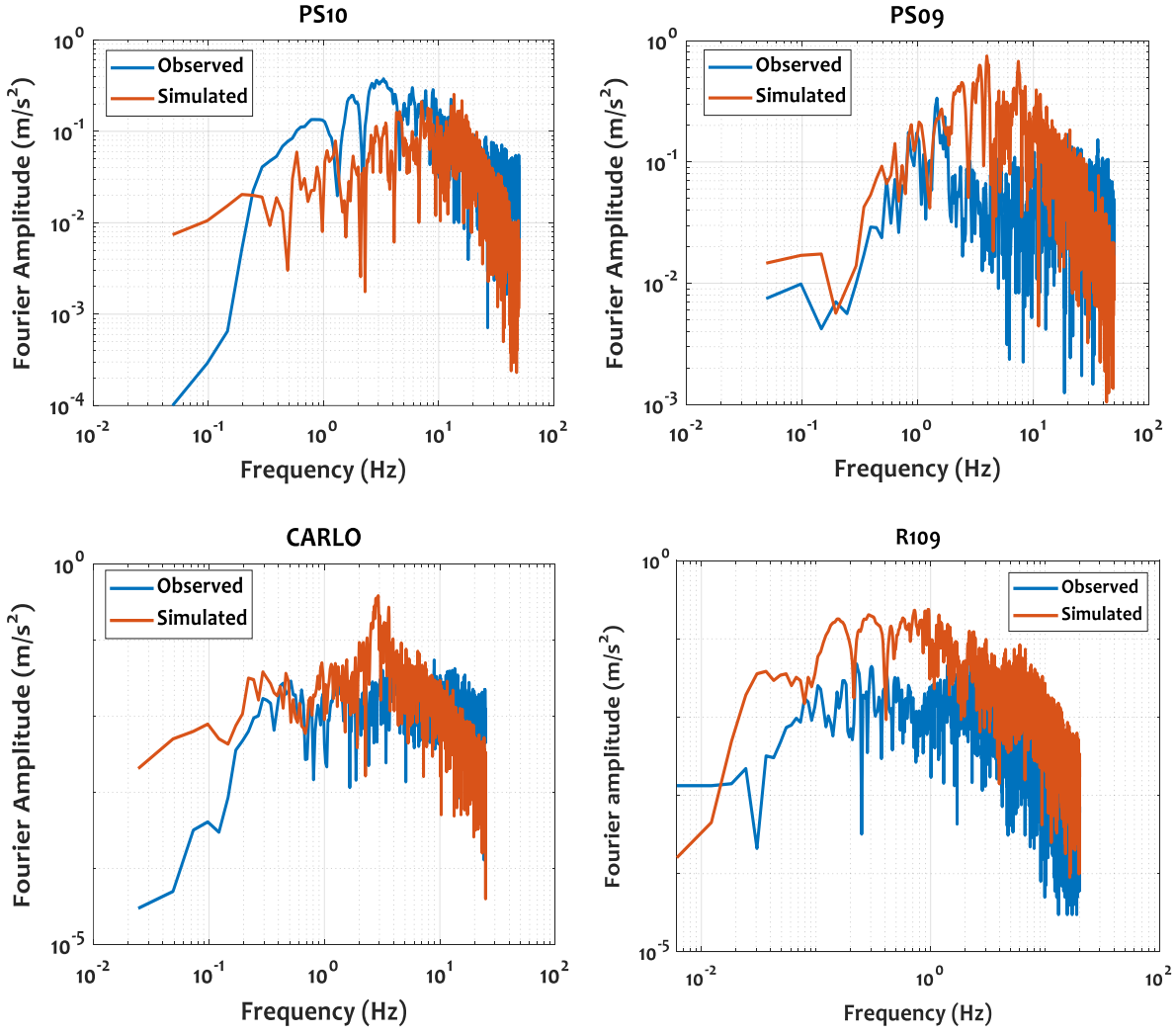

Fig. 4. Fourier amplitude spectra obtained through observed and simulated ground motions at PS10, PS09, CARLO and R109 stations during 2002 Denali earthquake

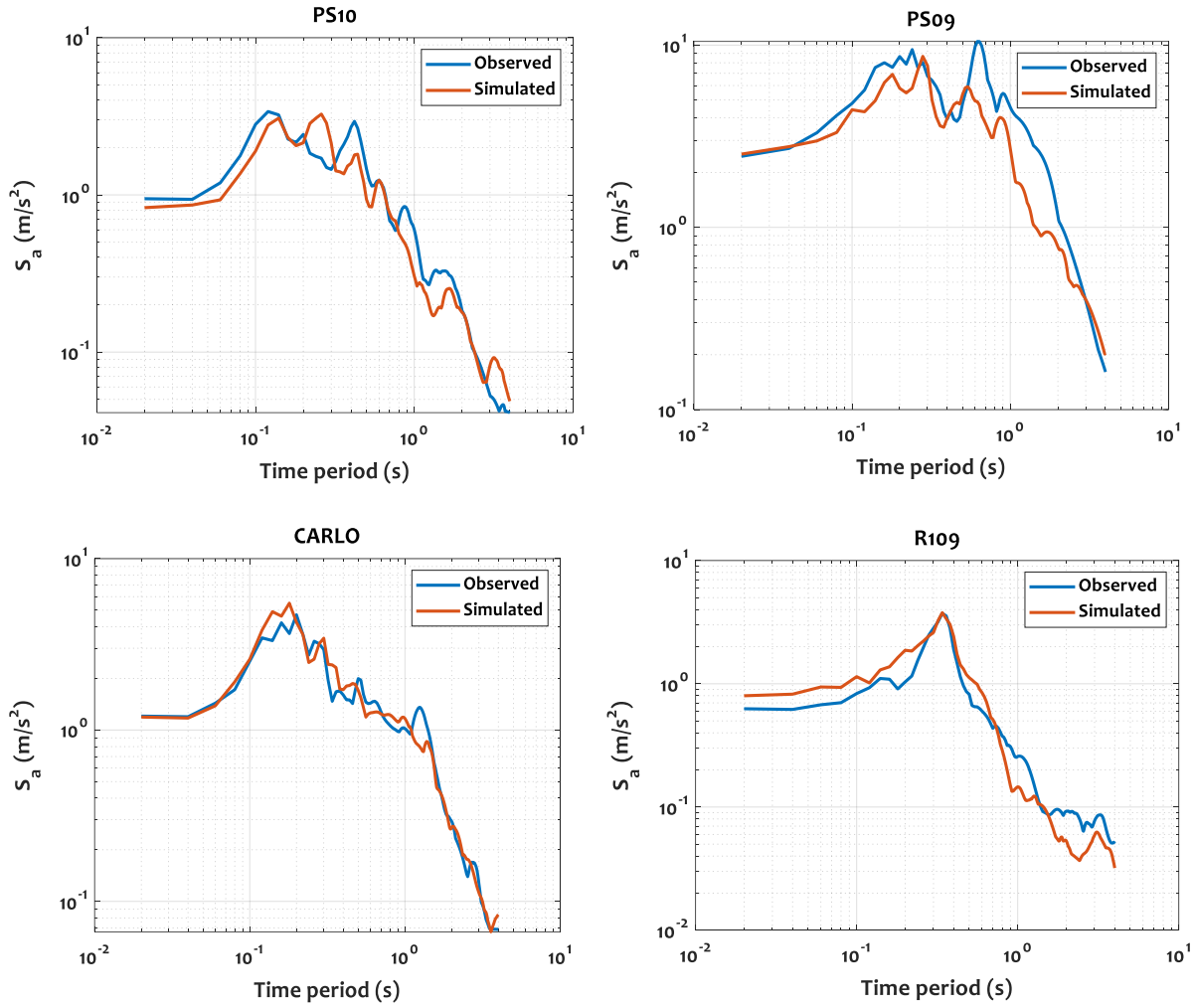

Fig. 5. Comparison of elastic acceleration response spectra between observed and simulated ground motions during 2002 Denali earthquake

Station PS10: Trans-Alaskan pipeline station 10 is located 3 km from the fault rupture of Denali fault and 85 km from the epicenter of the earthquake. The fault slipped 4-6 m horizontally and 0.5 m vertically at PS10 (Andrea and Chao, 2016; Wang et al., 2016). More than 0.3g PGA was recorded along both horizontal directions. It is observed that PGA, PGV and PGD of FN components are 1-30% higher than FP components. The corner frequency of Fourier amplitude is at 0.09 Hz and the decay starts at 1 Hz. High spectral acceleration on response spectrum is observed at a time period of 0.14 s.

Station PS09: Trans-Alaska pipeline station 09 is located 56 km from the fault rupture of Denali fault and 94 km from the epicenter of the earthquake. The fault slipped 4-6 m horizontally at PS09. Less than 0.1g PGA was observed along both horizontal directions. The corner frequency of Fourier amplitude is at 0.1 Hz and the decay starts at 1 Hz. High spectral acceleration on response spectrum is observed at a time period of 0.6 s.

Station CARLO: It is a temporary station located on the Denali highway, which is 59 km from the fault rupture of Denali fault and 68 km from the epicenter of the earthquake. The fault slipped 1 m horizontally at CARLO (Wang et al., 2016). Less than 0.1g PGA was observed along both horizontal directions. The corner frequency of Fourier amplitude is at 0.1 Hz and the decay starts at 1 Hz. High spectral acceleration on response spectrum is observed at a time period of 0.2 s.

Station R109: It is also a temporary station located on the Parks highway, which

is 49 km from the fault rupture of Denali fault and 63 km from the epicenter of the earthquake. The fault slipped 1 m horizontally at R109 (Wang et al., 2016). More than 0.05g PGA was observed along both horizontal directions. The corner frequency of Fourier amplitude is at 0.1 Hz and the decay starts at 1 Hz. High spectral acceleration on response spectrum is observed at a time period of 0.35 s.

4. Generation of Ground Motion Prediction Equation (GMPE) and Q Parameter

4.1. GMPE

The general functional form of GMPE is expressed in Ee. (1).

$$f(Y) = a + f_1(M) + f_2(R) + f_3(S) + \sigma \quad (1)$$

where *Y*: is predicted PGA, $f_1(M)$: is a function of magnitude of earthquake, $f_2(R)$: is a function of epicentral distance, $f_3(S)$: is a function of site categories like rock and soil sites, and σ: is a value of relating uncertainties in the predicted *f(Y)*. A detailed procedure for developing GMPE is given by Rajaram (2016).

The functional form for modeling the ground motion attenuation can be represented using Eq. (2).

$$\log_{10}(Y) = a + bM + c\log_{10}\sqrt{R^2 + h^2} + eS + \sigma \quad (2)$$

where σ: is the standard deviation of the logarithm of *Y*, *M*: is the magnitude, *R*: is the Epicentral distance, *h*: is a function of *M*, *S*: is site categories (1 for soil site and 0 for rock site) and *a*, *b*, and *e*: are regression analysis coefficients.

The dataset consists of 57 seismic station records in the Alaska for studying the GMPE relationship. The Alaskan earthquake information and ground motion records are taken from SMVDC (2013) (see Table 5). Since most of the seismic stations are located on rock site, the term $f_3(S)$ is taken as zero. The distribution of dataset used in this analysis is from the earthquakes with a magnitude range of 5-7.9 and an Epicentral distance range of 35-190 km. The distribution of magnitude and number of seismic stations with respect to epicentral distance is shown in Figure 6. The dataset consists of two orthogonal horizontal components of PGA values, the resultant value has been chosen for the purpose of analysis.

The coefficient '*c*' in Eq. (2), which is a negative value, means the attenuation rate with respect to Epicentral distance. In other words, it is a weighted average of *c*'s, each of which is obtained from a data set of one earthquake at all Epicentral distances. The coefficient '*c*' must be greater than 1.0 for the short period amplitude attenuation relation, since this term includes the geometrical spreading of body wave and inelastic attenuation. Hence, the analysis considered the weighted average of *c*'s for a fixed at all Epicentral distances. Similarly, the coefficient *b* means the amplitude increase rate with respect to magnitude at a fixed distance. In other words, it is a weighted average of *b*'s, each of which is obtained from a dataset at a particular distance range for all earthquakes. In this analysis, the weighted average of b and c are taken at all Epicentral distances and at all earthquakes, respectively.

Table 5. The Alaskan earthquake information and dataset (Data source: SMVDC, 2013)

Earthquake	Date	Mw	No. of stations
Southeastern Alaska	04 Jun 2014	5.7	3
Southern Alaska	22 Jun 2009	5.5	8
Nelchina	25 Aug 2004	5.3	3
Rampart	02 Apr 2003	5.0	1
Denali	03 Nov 2002	7.9	30
Nenana mountain	23 Oct 2002	6.7	5
SE Alaska	28 Feb 1979	7.4	3
Anchorage	01 Jan 1975	5.9	4

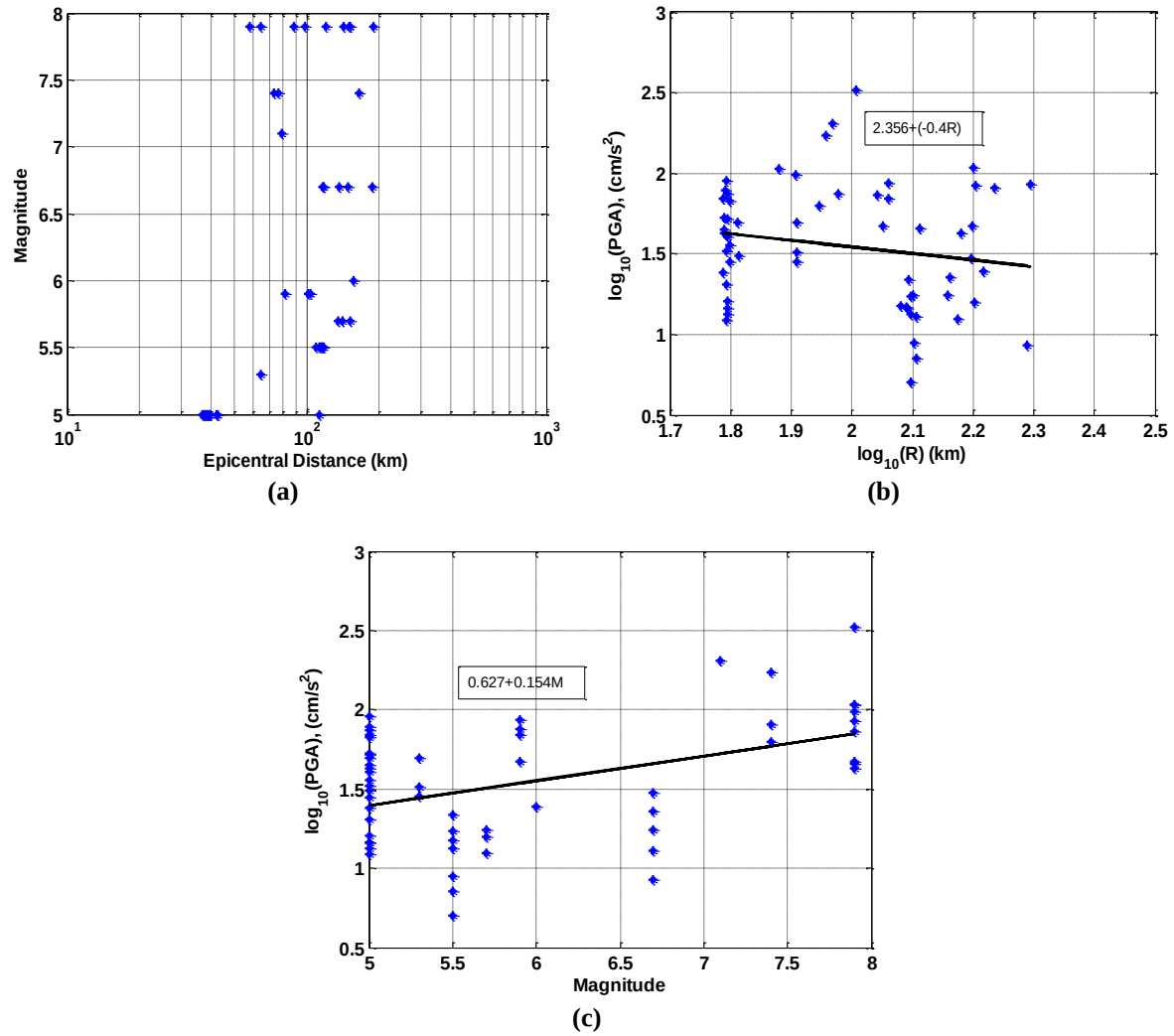

Fig. 6. Generation of GMPE: a) Distribution of magnitude and number of seismic stations with respect to Epicentral distance; b) Distribution of horizontal PGA to Epicentral distance; and c) Distribution of horizontal PGA to magnitude

The residual values represent the ratio of logarithmic of observed to predicted PGAs as shown in Eq. (3).

$$\text{Residual} = \log_{10}\left(\frac{Y_{\text{observed}}}{Y_{\text{predicted}}}\right) \quad (3)$$

where $Y_{observed}$: is the observed value from ground motion record (e.g. PGA), while $Y_{predicted}$: represents the value predicted by the GMPE. The regression coefficients are calculated using regression analysis. The GMPE obtained from the analysis is shown in Eq. (4), which resembles Hasegawa's GMPE, proposed for Canadian region in 1981 (Hasegawa et al., 1981). The GMPE in Eq. (4) considers a seismic catalog from 1971 to 2014, whereas Hasegawa considered from 1971 to 1981.

$$\log_{10}(Y) = 2.356 + 0.15M - 2.207\log_{10}\sqrt{R^2+h^2} + 0.243 \quad .....(5.0 \le M \le 8.0) \quad (4)$$

4.2. Frequency Dependent Q Parameter

There are several techniques to investigate site effects due to local site conditions. In general, *H/V* spectral ratio method is used to calculate the site effects. In general, Q is represented as $Q = Q_o f^n$, (Hajiazizi et al., 2021) where Q_o: is the Q value at 1 Hz and n varies from 0 to 1.

The procedure for estimating the Q factor is as follows:

- Collection of ground motion records for a region of interest. Convert all ground motion records into frequency domain.

- Computing the ratio of horizontal to vertical amplitude spectra and also compute average amplitude spectrum.
- Compute the *Q* parameter against frequency using Eq. (5).

$$\log_{10} A(R,f) - \log C - \log GS - \log F(f) = \log S(f) - 1.36\frac{fR}{\beta Q(f)} \quad (5)$$

where *C*: is a constant and *GS*: is geometrical spreading term. *F(f)*: is derived through *H/V* spectral ratio method shown in Figure 7. Hence at each frequency, the values of *Q(f)* and *S(f)* are obtained by fitting the above equation to the observed Fourier amplitude spectra shown in Figure 8.

- Estimation of *Q* parameter value for a region of interest through regression analysis (power law).

For the purpose of analysis, 57 ground motion records have been considered along three translational directions to plot *H/V* spectral ratio. The ground motion records are transformed into frequency domain using Fast Fourier Transform (FFT). The *H/V* spectrum is obtained as the ratio of vector summation of two horizontal component spectra along FN and FP components and vertical component spectral amplitude *V* at each frequency. The average *H/V* spectrum is obtained by arithmetic average of individual *H/V* spectra over all time windows. A plot is drawn between the *H/V* spectral ratio on the ordinates and the frequency on the abscissa. From the analysis, it is observed that the average amplification factor increases as the frequency increases till 0.15 Hz. Then it starts decreasing from 10 Hz. No significant amplification of *H/V* ratio is observed, as most of the ground motions are recorded on rock site. *Q* value is estimated from Eq. (5). It is found that the frequency dependent *Q* parameter for Alaska region is $Q(f) = 23.89f^{1.02}$. The parameters for generating synthetic accelerogram are derived for Alaskan region. The methodology and generation of synthetic accelerogram at stations through modified semi-empirical approach are as follows.

5. Generation of Ground Motions using Semi-Empirical Approach

The semi-empirical method was first developed by Midorikawa (1993). Later, the method was modified by Sandeep et al. (2015). The method is based on ω^2 model (Boore, 1983). A step-by-step procedure of the method is described below.

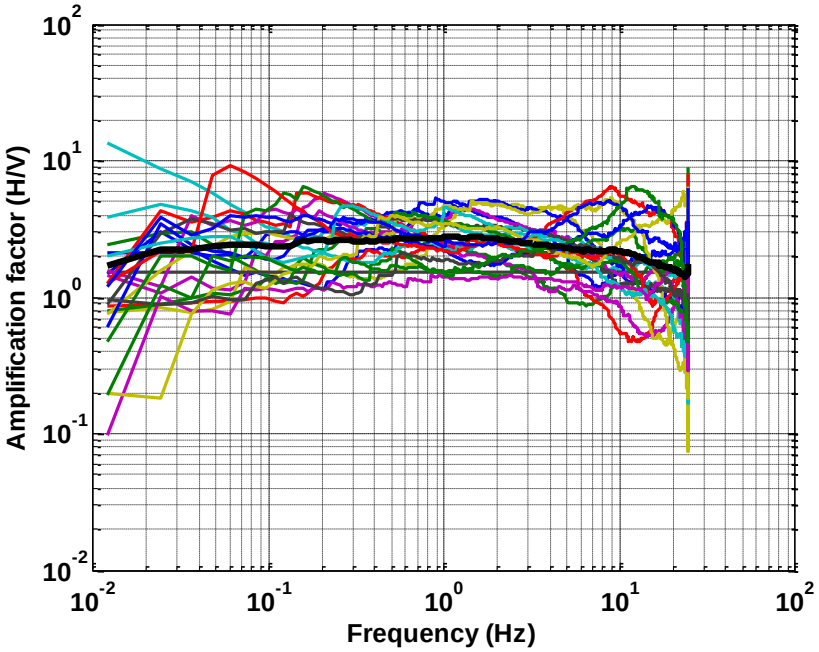

Fig. 7. Amplification of H/V for Alaska region

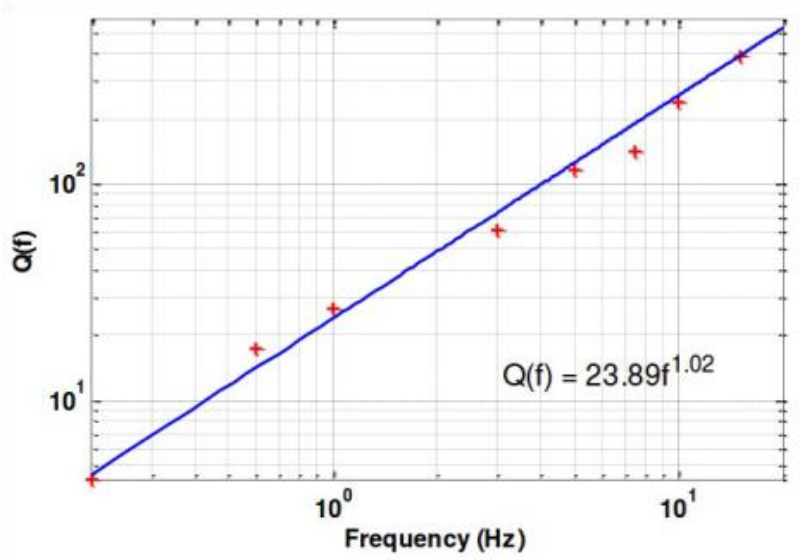

Fig. 8. Determination of Q parameter value for Alaska region

Step-1: Divide the fault plane into number of sub faults (*N*) based on scaling relationship between Richter magnitude of large (*M*) and small (*m*) earthquakes and Eq. (6) is as follows (Sato, 1989):

$$N = 10^{0.5(\mathrm{M-m})}. \quad (6)$$

Step-2: The white Gaussian noise is initially normalized and then converted to zero mean and variance. The time series of white Gaussian noise is converted into Fourier spectrum through Fourier transform and maintained maximum amplitude as unity.

Step-3: The amplitude spectrum is passed through theoretical filters proposed by Boore (1983) as shown in Eq. (7).

$$A(f) = \mathrm{CS(f)D_S(f)F_R(f,R)}. \quad (7)$$

where *C*: is a constant including seismic moment (M_o). The filter *S(f)*: represents the source acceleration spectrum (Javier et al., 2016), filter $D_S(f)$: represents near site attenuation of high frequencies, and filter $F_R(f,R)$: represents effect of anelastic attenuation.

Step-4: The filtered amplitude spectrum *A(f)* is again converted into time series *A(t)* and ensures the time series must be normalized. A correction function *F(t)* is introduced to minimize the difference between slip duration of the target and small earthquake considered (Krishnavajjhala, 2021). The correction function is calculated using Eq. (8).

$$F(t) = \delta(t) + [(N-1)/T_R(1-e^{-1})].e^{(-t/T_R)}. \quad (8)$$

where $\delta(t)$: represents delta function, and T_R: is the rise time of the target earthquake.

Step-5: Construction of acceleration envelope waveform $e_{ij}(t)$, modified by Sandeep et al. (2015) and Lal et al. (2018), is shown in Eq. (9).

$$e_{ij}(t) = \left[a_{ij} \frac{t}{T_d} e^{\left(1-\frac{t}{T_d}\right)} \right]; \quad \mathrm{E(t)} = \sqrt{\sum_{i=1}^{N}\sum_{j=1}^{N} e_{ij}^2 (t - t_{ij})}. \quad (9)$$

where a_{ij}: is the peak ground acceleration at each sub-fault obtain from ground motion prediction equations. T_d: represents duration parameter, t_{ij}: is the arrival time at observation point (Rajaram, 2016)

Step-6: The acceleration time history record at each sub-fault $A_{ij}(t)$ is calculated by multiplication of the envelope wave form e_{ij} with filtered white noise acceleration time history *A(t)*, and correction function *F(t)*. Eq. (10) is shown below:

$$A_{ij}(t) = e_{ij}(t).A(t).F(t) \quad (10)$$

Step-7: The summation of acceleration time history records at each sub-fault gives final acceleration record *AC(t)*. Further, it is resolved into two horizontal components along EW and NS directions.

The schematic diagram of modified semi-empirical approach is shown in Figure 9. The summary of modified semi-empirical approach for simulation of NS and EW component of earthquake ground motion is illustrated in Figure 10.

6. Results and Discussion

The modified semi-empirical method is implemented to generate synthetic accelerograms of the 03 November 2002 Denali earthquake. A MATLAB code earlier written, has been modified with correction function to obtain synthetic accelerograms at each station (Rajaram and Pradeep, 2016; MATLAB, 2018). A comparison study of PGA, duration, frequency, response spectra has been done between observed and simulated ground motions. The Fourier amplitude spectra and acceleration response spectra at all stations are shown in Figures 4 and 5. A comparison between PGA and duration of simulated and observed ground motions are shown in Figures 11 and 12. The synthetic accelerograms at selected stations are explained below:

Station PS10: The simulated accelerograms have lesser PGAs than observed accelerograms. The simulated PGA values are lesser than observed PGA values. A good match is observed between duration of simulated and observed ground motions. But, the Fourier amplitude spectrum overestimates the observed ground motion spectrum. A good match is observed between response spectra of observed and simulated ground motion.

Station PS09: The simulated accelerograms have higher PGAs than observed accelerograms. A good match is observed between duration of simulated and observed ground motions. The Fourier amplitude spectrum matches with observed ground motion spectrum. A good match is observed between response spectra of observed and simulated ground motion.

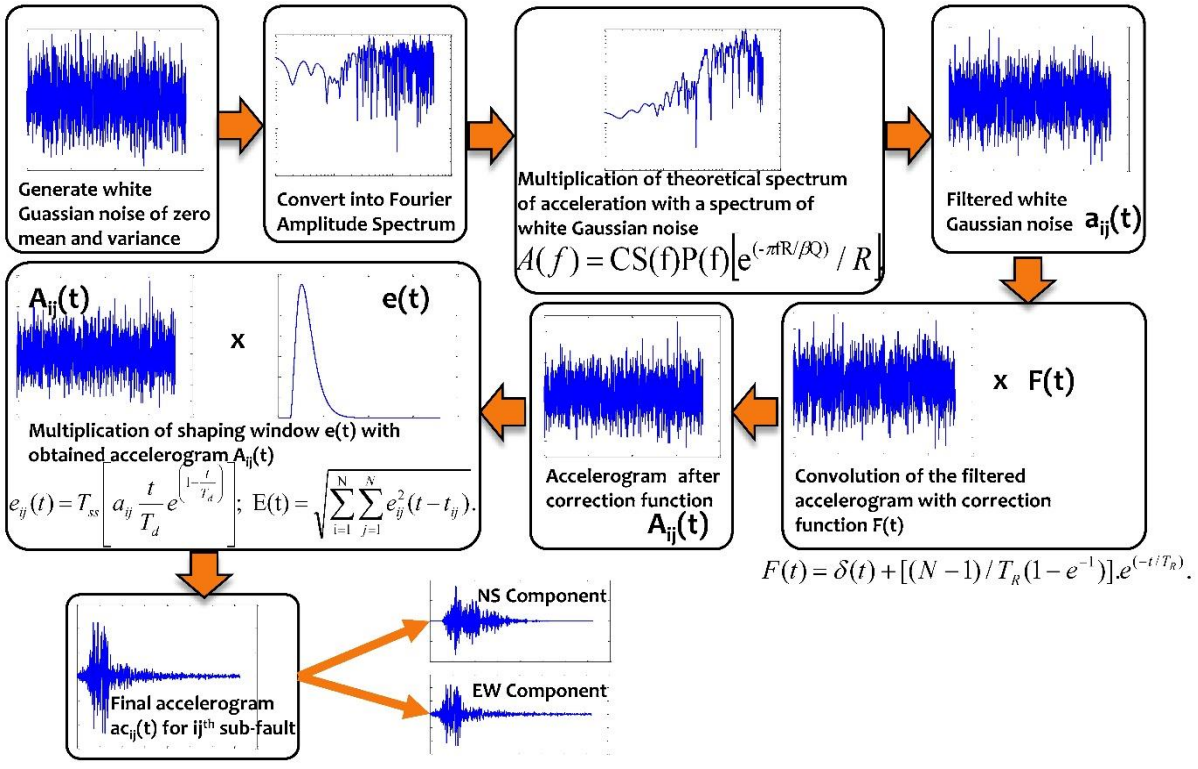

Fig. 9. Schematic diagram of modified semi-empirical approach

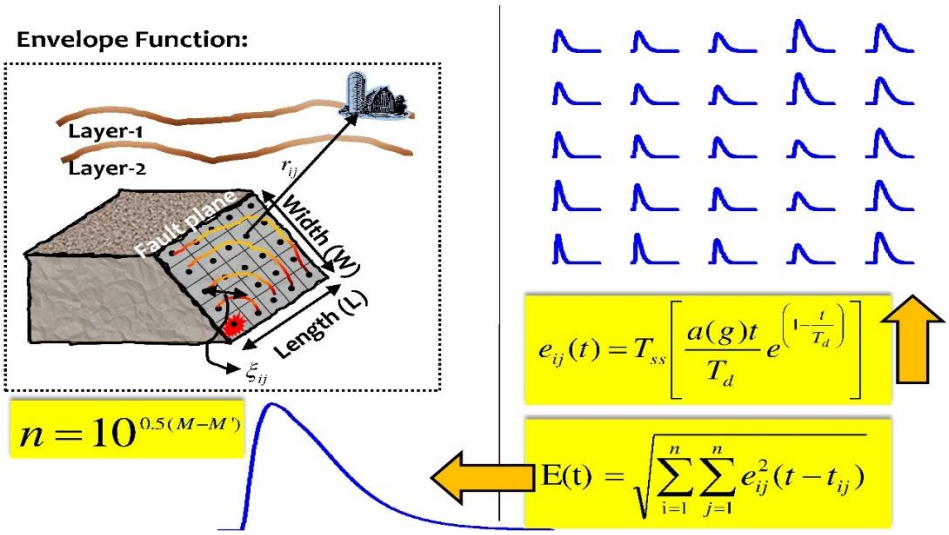

(a) Envelope function method

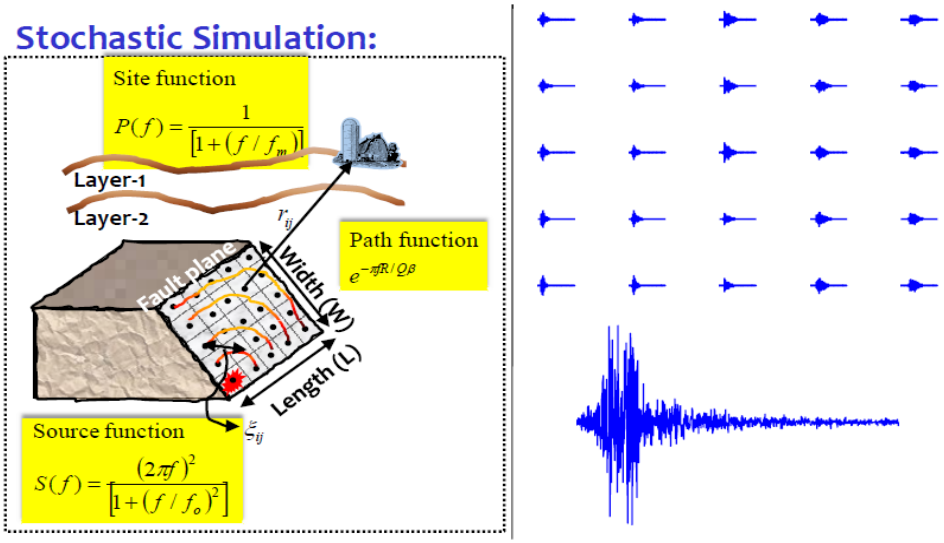

(b) Stochastic simulation method

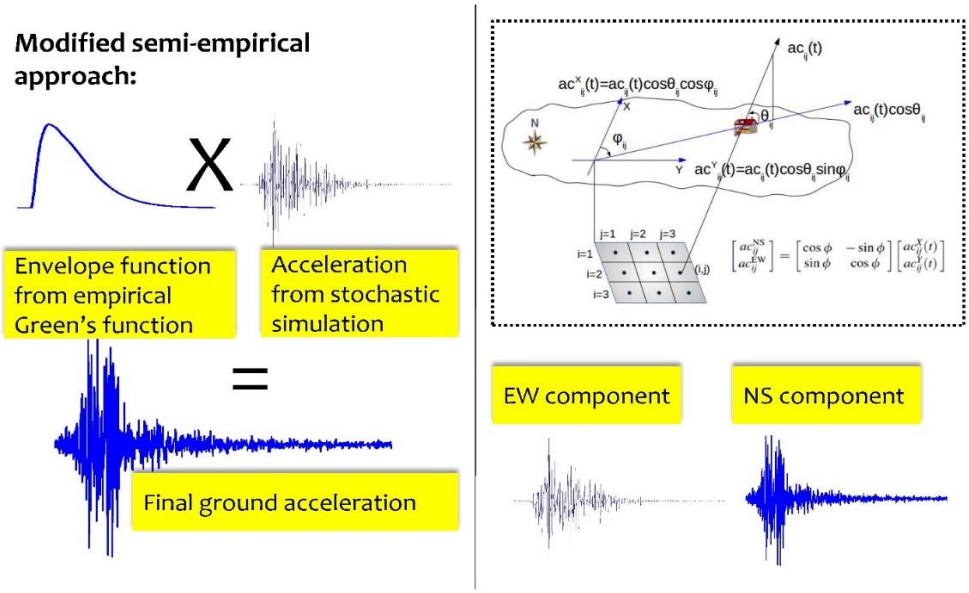

(c) Modified semi-empirical method

Fig. 10. Schematic diagram of: a) Envelope function method; b) Stochastic simulation method; and c) Modified semi-empirical method (combination of above methods)

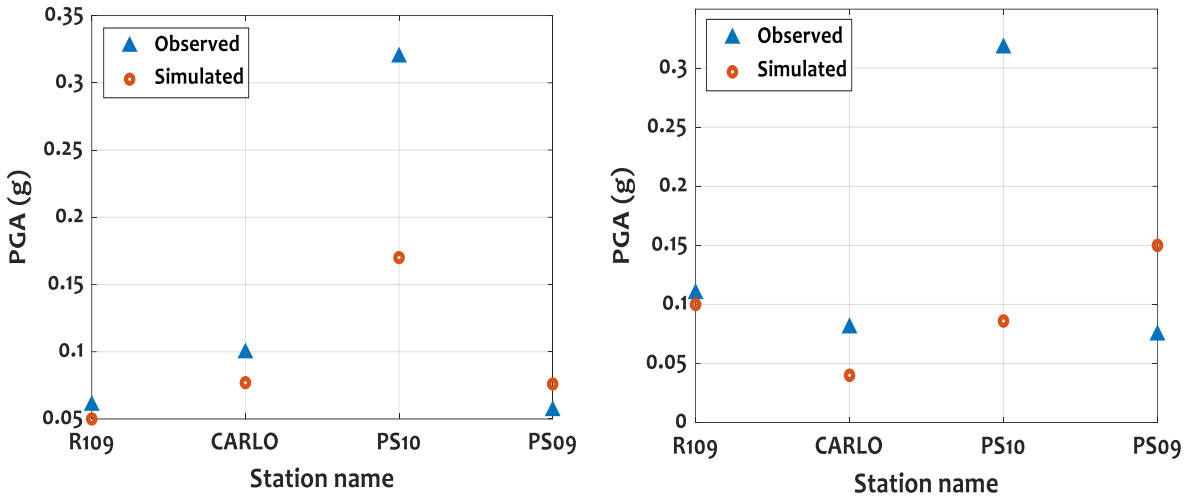

Fig. 11. Comparison of PGAs between observed and simulated ground motions during 2002 Denali earthquake: a) FP; and b) FN

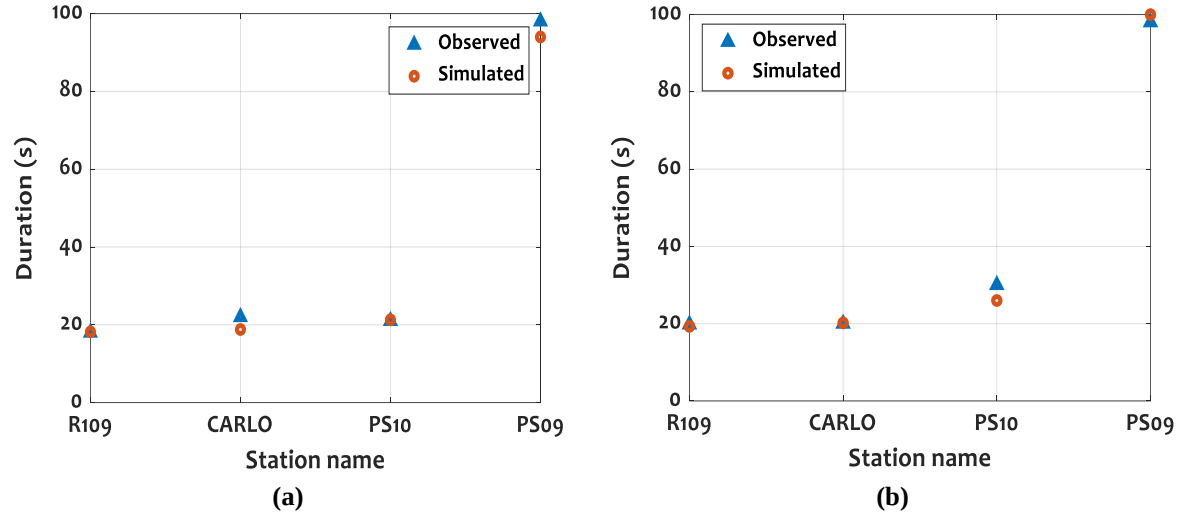

Fig. 12. Comparison of duration parameter between observed and simulated ground motions during 2002 Denali earthquake: a) FP; and b) FN

Station CARLO: The simulated accelerograms have lesser PGAs than observed accelerograms. A good match is observed between duration of simulated and observed ground motions. The Fourier amplitude spectrum matches with observed ground motion spectrum. A good match is observed between response spectra of observed and simulated ground motion.

Station R109: The simulated accelerograms have lesser PGAs than observed accelerograms. A good match is observed between duration of simulated and observed ground motions. The Fourier amplitude spectrum underestimates with observed ground motion spectrum. A good match is observed between response spectra of observed and simulated ground motion.

From the results, it is observed that the variation between observed and simulated ground motions is due to lack of seismicity, and ground motion record data. Envelope waveform function plays a vital role in semi-empirical simulation which is dependent on GMPE. The PGA and duration of simulated ground motion give satisfactorily results with observed ground motions. Also, a good match is observed between response spectra and Fourier amplitude spectra between observed and simulated ground motions.

7. Conclusions

In this study, a strike-slip Denali fault was considered for studying the characteristics of ground motions through modified semi-empirical approach. A MATLAB code was modified with correction function to generate ground motion records of 2002 Denali earthquake. For this purpose, four seismic stations PS10, PS09, CARLO and R109 were selected that recorded the 2002 Denali earthquake. The acceleration records were compared with observed acceleration records at the stations. From the above results, it is concluded that the results obtained from the proposed approach are good with observed ground motion records at all stations. The PGA values obtained from the prpos approach are nearer to the observed PGA values at CARLO and R109 stations. A perfect match is observed between Fourier amplitude spectra of the simulated and observed ground motions at PS09 and CARLO stations. The response spectra obtained from simulated ground motion matches with observed ground motions at all stations.

8. References

AEIC (Alaska Earthquake Information Center). (2019). http://earthquake.alaska.edu/

Anderson, J.G. (2015), "The composite source model for broadband simulations of strong ground motions", *Seismological Research Letters*, 86(1), 68-74.

Andrea, B. and Chao, L. (2016). "Near-field radiated wave field may help to understand the style of the super-shear transition of dynamic ruptures", *Physics of the Earth and Planetary Interiors*, 261, 133-140.

Boore, D.M. (1983). "Stochastic simulation of high frequency ground motion based on seismological models of radiated spectra", *Bulletin of Seismological Society of America*, 73, 1865-1894.

Consortium of Organizations for Strong-Motion Observation Systems (COSMOS). (2013), http://strongmotioncenter.org/vdc/scripts/earthquakes.plx, dated: 20 August 2013.

Dreger, D. (2003). "Finite source modeling of great earthquakes", Annual Report, Berkeley Seismological Laboratory, University of California, Berkeley, United States of America.

Hajiazizi, M., Taban, M.H. and Ghobadian, R. (2021). "Prediction of Q-value by multi-variable regression and novel Genetic Algorithm based on the most influential parameters", *Civil Engineering Infrastructures Journal*, 54(2), 267-280.

Hasegawa, H.S., Basham, P.W. and Berry, M.J. (1981). "Attenuation relations for strong seismic ground motion in Canada", *Bulletin of Seismological Society of America*, 71, 1943-1962.

Javier, L., Miguel, A.S., Miguel, A.J., Yanet, A. and Marcos, C. (2016). "Local earthquakes of the Mexico Basin in Mexico City: κ, Q, source spectra and stress drop", *Bulletin of the Seismological Society of America*, 106(4), 1423-1437.

Kikuchi, M. and Yamanaka, Y. (2002). "Source rupture processes of the central Alaska earthquake of Nov. 3, 2002, inferred from tele-seismic body waves", EIC Seismological Note 129, Earthquake Research Institute (ERI), University of Tokyo, Tokyo.

Krishnavajjhala, S. (2021). "Simulation of strong ground motion in the National Capital Region, India, from a future 8.5 magnitude earthquake using two-step empirical Green's function method", *Bulletin of Seismological Society of America*, 111(4), 1-18.

Lal, S., Joshi, A., Sandeep., Monu, T., Parveen, K., Chun-Hsiang, K., Che-Min, L., Kuo-Liang, W. and Sharma, M.L. (2018). "Modeling of the strong ground motion of 25th April 2015 Nepal earthquake using modified semi-empirical technique", *Acta Geophysica*, 66, 461-477.

Lin, Z., Liu, Z.J., Weldon, R.J., Tian, J., Ding, C. and Du, Y. (2020). "Modeling repeated co-seismic slip to identify and characterize individual earthquakes from geomorphic offsets on strike-slip faults", *Earth and Planetary Science Letters*, 545, 1-14.

MATLAB (2018). *The MathWorks, Inc.*, Natick, Massachusetts, United States of America.

Midorikawa, S. (1993). "Semi-empirical estimation of peak ground acceleration from large earthquakes", *Tectonophysics*, 218, 287-295.

Mobinipour, S.A. and Pourzeynali, S. (2020). "Assessment of near-fault ground motion effects on the fragility curves of tall steel moment resisting frames", *Civil Engineering Infrastructures Journal*, 53(1), 71-88.

Ozacar, A.A. and Beck, S.L. (2004). "The 2002 Denali fault and 2001 Kunlun fault earthquakes: Complex rupture processes of two large strike-slip events", *Bulletin of Seismological Society of America*, 94, S278-S292.

Rajaram, C. and Pradeep R.K. (2020). "Preliminary estimation of ground motion of September 24, 2013, Pakistan earthquake using modified semi-empirical approach", *Journal of Seismology and*

Earthquake Engineering, 22, 1-12.

Rajaram, C. (2016). "Numerical modeling of near fault seismic ground motions for strike-slip and dip-slip faults", Ph.D. Thesis, International Institute of Information Technology, Hyderabad, India.

Rajaram, C. and Pradeep R.K. (2016). "Simulation of near-field ground motion characteristics of May 01, 2013, Doda earthquake using modified semi-empirical approach", *Natural Hazards*, 82, 1411-1430.

Ratchkovski, N.A., Hansen, R.A., Stachnik, J.C., Cox, T., Fox, O., Rao, L., Clark, E., Lafevers, M., Estes, S., MacCormack, J.B. and Williams, T. (2003). "Aftershock sequence of the Mw 7.9 Denali fault, Alaska, earthquake of 3 November 2002 from regional seismic network data", *Seismological Research Letters*, 74, 743-752.

Sandeep, A., Joshi, A., Kamal, P., Kumar, A. and Kumar, P.D. (2015). "Modeling of strong motion generation areas of the Niigata, Japan, earthquake of 2007 using modified semi empirical technique", *Natural Hazards*, 77, 933-957.

Sandeep, A., Joshi, A., Lal, S., Kumar, P. and Sah, S.K. (2017). "Simulation of strong ground motion of the 2009 Bhutan earthquake using modified semi-empirical technique", *Pure and Applied Geophysics*, 174(12), 4343-4356.

Sato, R. (1989). *Handbook of fault parameters of Japanese earthquakes*, Kajima, Tokyo (in Japanese).

Strong Motion Virtual Data Centre (SMVDC). (2015), http://strongmotioncenter.org/vdc/scripts/earthquakes.plx, dated: 20 August 2015.

Tadahiro, K., Olga, J.K., Robert, B.D. and Walter, J.S. (2016). "Semi-automated procedure for windowing time series and computing Fourier amplitude spectra for the NGA-West2 database", PEER Report No. 2016/02, Pacific Earthquake Engineering Research Center, University of California, Berkeley, CA.

Uenishi, K. (2017). "Rupture, waves and earthquakes", *Proceedings of the Japan Academy Series B: Physical and Biological Sciences*, 93(1), 28-49.

United States Geological Survey (USGS). (2019). https://www.usgs.gov/ dated: 24 April 2019.

Wang, D., Mori, J. and Koketsu, K. (2016). "Fast rupture propagation for large strike-slip earthquakes", *Earth and Planetary Science Letters*, 440, 115-126.

Yousef, B. and Jonathan, P.S. (2020). "Data resources for NGA-subduction project", PEER Report No. 2020/02, Pacific Earthquake Engineering Research Center, University of California, Berkeley, CA.